A Force and Displacement Self-Sensing Piezoelectric MRI-Compatible Tweezer End Effector with an On Site Calibration Procedure

Timothy McPherson and Jun Ueda

***Abstract*—This work describes a self-sensing technique for a piezoelectrically driven MRI-compatible tweezer style end effector, suitable for robot assisted, MRI guided surgery. Nested strain amplification mechanisms are used to amplify the displacement of the piezo actuators to practical levels for robotics. By using a hysteretic piezoelectric model and a two port network model for the compliant nested strain amplifiers, it is shown that force and displacement at the tweezer tip can be estimated if the input voltage and charge are measured. One piezo unit is used simultaneously as a sensor and an actuator, preserving the full actuation capability of the device. An on site calibration procedure is proposed that calibrates the combined electromechanical model without requiring specific loading conditions on the inner piezoelectric actuators. Experimental validation shows an average of 12% error between the self-sensed and true values.**

***Index Terms*—Piezoelectric actuation, Self-Sensing, MRI Compatibility, Robotic End Effector.**

I. Introduction

ROBOT assisted surgery has quickly become a highly active field of research and is beginning to enter mainstream medicine with the success of the Da Vinci robot, developed by Intuitive Surgical Inc. [1]. Concurrently, research has been undertaken in magnetic resonance imaging (MRI) guided surgery [2] [3] [4] [5]. The combination of these two fields has the potential to improve patient outcomes by allowing an increasing number of procedures to be completed in a minimally invasive way. To that end, the investigation of new actuation and sensing strategies that are MRI compatible is needed to bring robotics into the MRI environment. Recently a MRI compatible tweezer style end effector suitable for robotic surgery has been devloped by Kurita et al., and is the starting point of this research [6].

Self-sensing actuation, or simultaneous actuation and sensing, is a technique that takes advantage of the unique properties of piezoelectric materials not only to use them as sensors, but to also simultaneously produced forces and displacements. This is achieved by using a specially designed circuit. This concept was originally proposed by Dosch et al. [7]. A bridge circuit was developed by placing capacitances in series and parallel with the piezoelectric actuator that produced a voltage output proportional to velocity or force. The method was subsequently refined and applied by other researchers [8] [9]. The three main drawbacks of the method are 1) that the operation of the bridge circuit requires close matching of the piezo capacitance, 2) only dynamic (i.e., vibration) measurements are possible, and 3) the hysteresis of the material is neglected. More recent work has addressed some of these issues by developing methods based on charge measurement, but make limiting assumptions, such as zero force or zero displacement on the actuator, and do not directly model hysteresis [10] [11] [12]. New models have also been developed to take hysteresis into account [13] [14]. As explained in [13], hysteresis is observed between voltage and charge but not charge and displacement, which suggests that the hysteresis occurs in the electrical domain. This means that for quasistatic operation charge is linearly related to displacement if there is zero external force on the actuator, or vice versa, so the linear model can appear correct. If one attempts to extend this model to a self-sensing scheme with unknown loading conditions, it is quickly seen that a model considering hysteresis is needed.

Badel et al. use the hysteretic model of [13] to achieve this, as well as implementing force control based on the self-sensed measurement [15]. In this work, calibration of the hysteretic model required two extreme loading conditions, namely, fully blocked and fully free. These loading conditions are easily be realizable in piezoelectric actuators when used as-is, but cannot be replicated in built-in actuators including amplified PZT actuators. This paper will show that intricate coupling between parameters in the mathematical model makes it difficult to calibrate the hysteresis model. Kurita et al. investigated the sensing problem for a tweezer-style end effector, and proposed using one actuator out of serially-connected actuators solely as a sensor [6]. Their results were promising, but the hysteresis was not modeled and the loading condition at the tip needed be known a priori. Consequently, there is no existing method that provides means to calibrate the electromechanical hysteresis of amplified PZT actuators.

In this paper, a new on site calibration procedure will be presented that does not require specific loading conditions on the piezo actuator. A self-sensing technique is attractive because it does not sacrifice actuation capability. An on-site calibration procedure is developed based on a mathematical model with a hysteretic piezoelectric model and a two-port network model of the compliant amplified PZT actuators. This formalism reveals mathematical insights that lead to an effective calibration procedure. Although this paper focuses on the robotic surgery application, the results can be used for vibration suppression devices for aircraft wings, piezo controlled engine valves, tip-tilt mirror positioners, and other

T. McPherson and J. Ueda are with the George W. Woodruff School of Mechanical Engineering, Georgia Institute of Technology, Atlanta, GA, 30332 USA e-mail: tmcpherson3@gatech.edu, jun.ueda@me.gatech.edu.

Manuscript received July 27, 2012; revised December 16, 2012.

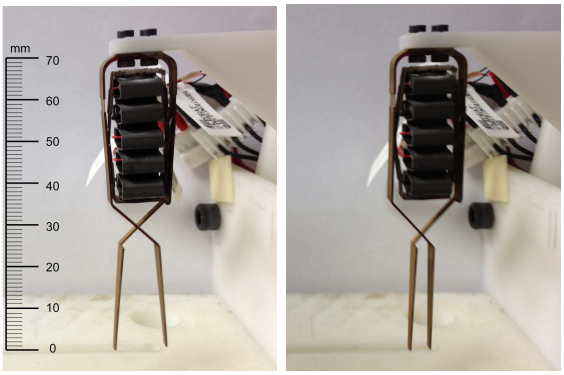

(a) Open (b) Closed

Fig. 1. Fully assembled tweezer structure. The tweezers arms act as the third layer of amplification.

types of micromanipulators, in which amplified PZT actuators are already in use.

II. Tweezer Structure

Piezoelectric actuators produce extremely small strain but comparatively large force. For robotic applications, larger displacements can be achieved by trading off force with amplification mechanisms, such as the rhomboidal mechanism. By nesting several of such mechanisms inside each other, strain rates of up to 20% can be achieved with sufficient force [16]. Using this principle, piezoelectrically driven tweezers were developed with three layers of strain amplification [6]. The first layer is made up of five commercially available Cedrat APA35XS piezoelectric actuators. The APA35XS consists of a multilayer Lead Zirconate Titanate (PZT) stack actuator surrounded by a single rhomboidal strain amplifier. These actuators are surrounded by a second amplification mechanism. Finally, the lever action of the tweezer arms themselves provide a third layer of amplification. The fully assembled tweezer device is shown in Fig.1. The tweezers produce 0.1 N of pinching force when fully blocked or 7 mm of displacement when fully free, and require a supply voltage of 0 to 150 V. Detailed information on the development of this device is found in [6]. Note that the force produced is lower than the previous version of the device due to manufacturing difficulties. Future versions of the device are expected to produce 1 N of pinching force as reported in [6].

Under quasistatic operation, a rhomboidal strain amplifier can be represented by a two port network model of the form [16]

$$\begin{bmatrix} f_{pzt} \\ f_1 \end{bmatrix} = \begin{bmatrix} s_1 & s_3 \\ s_3 & s_2 \end{bmatrix} \begin{bmatrix} \Delta x_{pzt} \\ \Delta x_1 \end{bmatrix} \quad (1)$$

Forces and displacements are defined as shown in Fig. 2. The parameters of the model can be interpreted intuitively as follows. s_1 is the stiffness at the input when the output is blocked. s_2 is the stiffness at the output when the input is blocked. Finally, s_3 is the ratio of force produced at the blocked output to a given input displacement. The second and third amplification layers amplification layers can be similarly represented by two port networks, as described in [6]. Schematic diagrams are shown in Fig. 3 and Fig 4.

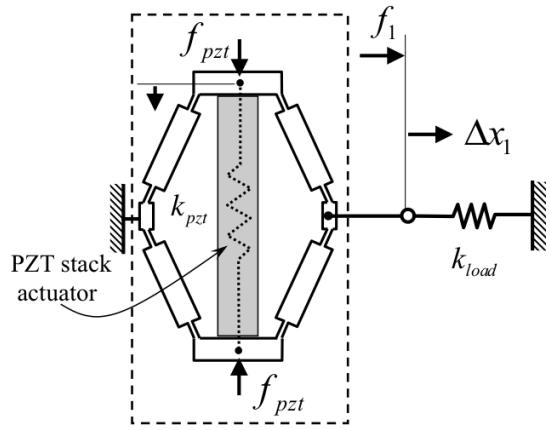

Fig. 2. Schematic diagram of a rhomboidal strain amplifier. A small input displacement Δx_{pzt} is amplified at the output, Δx_1.

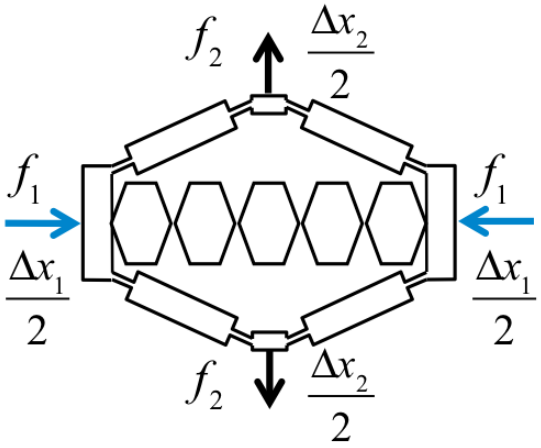

Fig. 3. Schematic representation of second amplification layer. Five actuators in series that drive the input of the second layer.

The input-output behavior of nested rhomboidal strain amplifiers can be represented by single, combined two port network if every layer is represented by a two port network [16]. However, it is not immediately obvious how to account for the five actuators in series that drive the input of the second layer. The question arises, can five rhomboidal strain amplifiers connected in series also be represented by a single two port network model? If so, the input-output relationship of the tweezer mechanism as a whole could be assumed to be a two port network. Consider Fig. 5 and Fig. 6. We assume that each strain amplifier sees an identical input since the PZT actuators are connected electrically in parallel. When the output is blocked, we have the equivalent of five springs in parallel at the input, meaning the effective s_1 would be five times that of a single rhomboid. When the input is blocked, the rhomboids act as springs in series in the output direction, so the effective s_2 is one fifth that of a single rhomboid. Finally, when the output is blocked, a given input displacement will create the same output force for a singe rhombus as for five in series. The reaction forces at connection points cancel, leaving the output force unchanged. It is now seen that the series connection of five actuators can be modeled with a single two

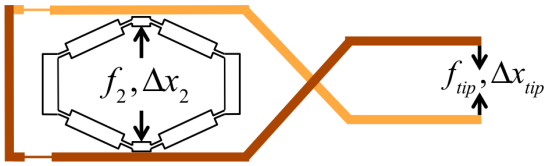

Fig. 4. Schematic representation of the tweezer arms and second amplification layer. The output of the second layer drives and input and the lever action of the tweezer arms provides the final layer of strain amplification.

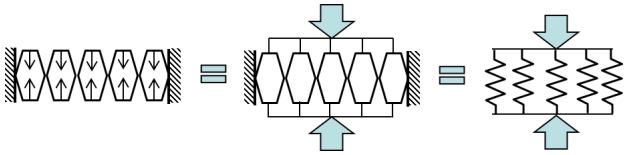

Fig. 5. Mechanical analysis of five rhomboids in series, output blocked.

Fig. 6. Mechanical analysis of five rhomboids in series, input blocked.

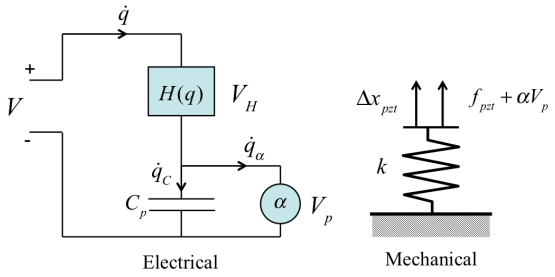

Fig. 7. Piezoelectric Actuator Model

port network. The input force to the combined model is $5f_{pzt}$ and the input displacement is Δx_{pzt}, since the five PZT stack actuators act in parallel on the input.

Recall that if each layer of the device can be written as a two port network, which was just shown, the entire device can be modeled by a single two port network model. This gives

$$\begin{bmatrix} f_{pzt} \\ n_A f_{tip} \end{bmatrix} = \begin{bmatrix} S_1 & S_3 \\ S_3 & S_2 \end{bmatrix} \begin{bmatrix} \Delta x_{pzt} \\ \Delta x_{tip} \end{bmatrix} \tag{2}$$

where S_1,S_2, and S_3 are the parameters describing the combined effects of all three amplification layers. n_A is the number of actuators connected in series, five in this case. This equation can then be rearranged to give outputs in terms of inputs.

$$\begin{bmatrix} \Delta x_{tip} \\ f_{tip} \end{bmatrix} = \begin{bmatrix} \dfrac{-S_1}{S_3} & \dfrac{1}{S_3} \\ S_3 - \dfrac{S_1 S_2}{S_3} & \dfrac{S_2}{S_3} \end{bmatrix} \begin{bmatrix} \Delta x_{pzt} \\ n_A f_{pzt} \end{bmatrix} \tag{3}$$

III. Electromechanical Modeling of Piezoelectric Actuators

Piezoceramics are known to exhibit pronounced hysteresis, and this effect is evident in Fig. 8. Note that the nonlinearity becomes greater with larger inputs, leading to the creation of minor loops inside the major loop that represents the full input output range. The electromechanical model proposed by Goldfarb and Celanovic is now widely in use to model this behavior [13]. A schematic representation of the model is shown in Fig. 7. The model describes the hysteric behavior of the actuator in addition to the electrical-mechanical interplay caused the direct and converse piezoelectric effects. The model is described by (4) through (7).

$$q = \alpha \Delta x_{pzt} + C_p V_p \tag{4}$$

$$V_H = H(q) \tag{5}$$

$$\frac{\Delta x_{pzt}}{f_{pzt} + \alpha V_p} = \frac{1}{k} \tag{6}$$

$$V = V_p + V_H \tag{7}$$

q is electric charge, V is the input voltage supplied to the actuator, α is the transformer ratio of the actuator with units of N/V, C_p is the clamped capacitance of the actuator, F is the external force, and k is the short circuit stiffness of the actuator. $H(q)$ is an operator modeling hysteresis and creep, as seen in Fig. 8,

Many phenomenological hysteresis models exist that can be used to define $H(q)$, such as the Prandtl-Ishlinskii operator [17], Preisach operator [18], Generalized Maxwell Slip Operator [13], and differential equations method [19]. The modified Prandtl-Ishlinkii approach developed by Kuhnen in [20] is used here due to several useful advantages, such as the ability to model asymmetric loops and minor loops, an automatic identification procedure, and extendability to creep modeling. It is based on the weighted summation of elementary play, superposition, and creep operators. Identification of weights can be formulated as a quadratic programming problem, described in detail in [20]. In short, one experiment is required to generate an input-output relationship. The weights are then optimized by a numerical search such that they minimize the error squared between model and experiment.

IV. Self-Sensing Technique

A. Combined Electromechanical Model of the Tweezer Device

Equations (4) and (6) can be written in matrix form, shown in (8).

$$\begin{bmatrix} \Delta x_{pzt} \\ f_{pzt} \end{bmatrix} = \begin{bmatrix} \dfrac{1}{\alpha} & \dfrac{-C_p}{\alpha} \\ \dfrac{-k}{\alpha} & \alpha + \dfrac{C_p k}{\alpha} \end{bmatrix} \begin{bmatrix} q \\ V_p \end{bmatrix} \tag{8}$$

Note we have negated F since we wish to represent the force supplied by the PZT actuator rather than the external force on the actuator, since the latter is the input to the two port network model representing the tweezers. Combining (8) with (3) the force and displacement at the tip can be written in terms of q and V_p. Note that the matrix of (8) has been modified to reflect that connection of actuators electrically in parallel, but constants α, C_p, and k are with respect to a single actuator. For n_A actuators connected in parallel, α, C_p, and k will all increase by a factor of n_A, which is reflected in (9). Additionally the charge will be n_A times that of a single actuator. As described earlier, here n_A is five. By noticing the

$$\begin{bmatrix}\Delta x_{tip}\\ f_{tip}\end{bmatrix} = \begin{bmatrix}\dfrac{-S_1}{S_3} & \dfrac{1}{S_3}\\ S_3 - \dfrac{S_1S_2}{S_3} & \dfrac{S_2}{S_3}\end{bmatrix}\begin{bmatrix}\dfrac{1}{n_A\alpha} & \dfrac{-C_p}{\alpha}\\ \dfrac{-k}{\alpha} & n_A\alpha + \dfrac{n_AC_pk}{\alpha}\end{bmatrix}\begin{bmatrix}n_Aq\\ V_p\end{bmatrix}$$
$$= \begin{bmatrix}\dfrac{-n_Ak - S_1}{n_AS_3\alpha} & \dfrac{n_AC_pk + C_pS_1 + n_A\alpha^2}{S_3\alpha}\\ \dfrac{S_2(-n_Ak - S_1) + S_3^2}{n_AS_3\alpha} & \dfrac{S_2(n_AC_pk + C_pS_1 + n_A\alpha^2) - CpS_3^2}{S_3\alpha}\end{bmatrix}\begin{bmatrix}n_Aq\\ V_p\end{bmatrix} \quad (9)$$

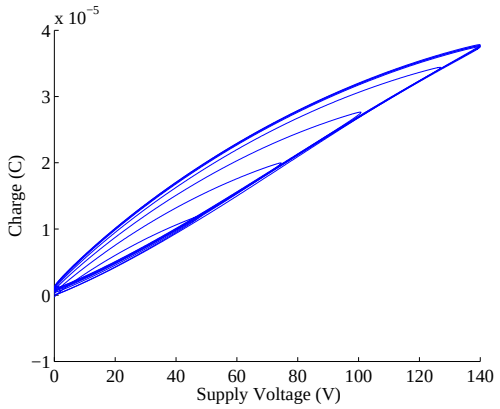

Fig. 8. Hysteresis between input voltage and charge of the middle actuator of five in the tweezer device. The loops are traversed counterclockwise with increasing voltage. Note the minor loops that form when the input voltage range is smaller.

similarity between the first and second rows of the matrix, (9) can be expressed as

$$\begin{bmatrix}\Delta x_{tip}\\ f_{tip}\end{bmatrix} = \begin{bmatrix}A_1 & A_2\\ S_2A_1 + S_3/n_A\alpha & S_2A_2 - C_pS_3/\alpha\end{bmatrix}\begin{bmatrix}n_Aq\\ V_p\end{bmatrix} \quad (10)$$

where A_1 and A_2 are defined by

$$A_1 = \frac{-n_Ak - S_1}{n_AS_3\alpha} \quad (11)$$

$$A_2 = \frac{n_AC_pk + C_pS_1 + n_A\alpha^2}{S_3\alpha} \quad (12)$$

Recalling that $V_p = V - H(q)$, it is now seen that the force and displacement at the tweezer tip can be sensed simultaneously if the driving voltage, charge, and hysteresis operator $H(q)$ are known.

B. Model Parameter Identification

In prior work on piezoelectric modeling and self-sensing, identification of model parameters has been relatively straightforward [13] [15]. However, the addition of strain amplification mechanisms complicates the matter. For a singular, unamplified PZT actuator, the parameters α, k, and C_p, and the hysteresis operator $H(q)$ can be identified by taking three measurements, namely the maximum force generated by the blocked actuator, the maximum displacement of the free actuator, and the charge vs. voltage profile of the free actuator as the input voltage is varied from it's minimum to maximum value [15]. When the PZT actuator is nested inside several layers of strain amplification, it is impossible to recreate the necessary loading conditions, so a different approach is taken.

The parameters S_1, S_2, and S_3 can be estimated by the following equations [16].

$$S_1 = \frac{f_{pzt}^{block}}{\Delta x_{pzt}^{block}} \quad (13)$$

$$S_2 = \frac{\Delta x_{pzt}^{free}}{\Delta x_{tip}^{free}}\frac{f_{tip}^{block}}{\Delta x_{pzt}^{block}} \quad (14)$$

$$S_3 = -\frac{f_{tip}^{block}}{\Delta x_{pzt}^{block}} \quad (15)$$

Recall f_{pzt} and Δx_{pzt} are the input force and displacement supplied by the PZT actuator, while f_{tip} and Δx_{tip} are the force and displacement at the tweezer tip.The superscript *block* or *free* indicates the loading condition at the tweezer tip when the measurement is taken. As discussed above, f_{tip} and Δx_{tip} can be measured easily, while f_{pzt} and Δx_{pzt} must be estimated from catalog data. Catalog data can also be used to estimate α, k, and C_p. However, it is desirable to reduce the number of model parameters to calibrate, especially for those which depend on difficult to measure quantities. To this end, consider the case of the free tweezer tip, i.e. $f_{tip} \equiv 0$.

In this case we have

$$0 = f_{tip} = (S_2A_1n_Aq + S_2A_2V_p) + \left(\frac{S_3}{\alpha}q - \frac{C_pS_3}{\alpha}V_p\right) \quad (16)$$

Notice that

$$(S_2A_1n_Aq + S_2A_2V_p) = S_2\Delta x_{tip} \quad (17)$$

and that

$$S_2 = -\frac{\Delta x_{pzt}^{free}}{\Delta x_{tip}^{free}}S_3 \quad (18)$$

This gives

$$0 = \frac{S_3}{\alpha}(q - C_qV_p) - \beta S_3\Delta x_{tip} \quad (19)$$

where

$$\beta = \frac{\Delta x_{pzt}^{free}}{\Delta x_{tip}^{free}} \quad (20)$$

The term S_3 can then be canceled and the equation rearranged to yield an expression for V_p.

$$V_p = \frac{q}{C_p} - \frac{\alpha\beta}{C_p}\Delta x_{tip} \quad (21)$$

TABLE I
MODEL PARAMETERS FOR CALIBRATION OF $H(q)$

α	2.35 N/V
β	1.59 $\times 10^{-3}$
C_p	0.3 µF
A_q	84 m/C
Δx_{pzt}^{free}	10 µm
Δx_{tip}^{free}	6.3 mm

Combining (21) with (5) and (7) gives

$$H(q) = V - \frac{q}{C_p} + \frac{\alpha\beta}{C_p}\Delta x_{tip} \tag{22}$$

Therefore knowledge of C_p, Δx_{tip}, α, Δx_{pzt}^{free}, and Δx_{tip}^{free} are required to calibrate $H(q)$. C_p and Δx_{tip} can be measured directly, while α and Δx_{pzt} can be determined from published catalog data. Once $H(q)$ is known, A_1, A_2, $S_2A_1 + S_3/n_A\alpha$, and $S_2A_2 - C_pS_3/\alpha$ can be easily determined by regression.

One further simplifying step can be taken. When the tweezer tip is free, Δx_{tip} is directly proportional q [13]. Therefore once the appropriate scale factor A_q is determined, one can write

$$H(q) = V - \frac{1}{C_p}\left(1 - \alpha\beta A_q\right) q \tag{23}$$

This is beneficial because after initial determination of A_q the displacement measurement is not needed to calibrate $H(q)$. The model parameters in (23) are shown in Table I [21].

V. EXPERIMENTAL VALIDATION

A. Hardware and Setup

The inputs to the sensing model are charge and voltage. The actuators are driven by a Cedrat CA45 high voltage amplifier. The amplifier shows good linearity up to 500 Hz, well above the quasistatic operation considered here. This means that in practice the supply voltage does not need to be measured directly, but can be assumed as the amplifier gain times the input voltage to the amp. This eliminates the need for high voltage measurement equipment. The voltage across the actuator is given by

$$V = V_c - V_s \tag{24}$$

Charge can be accurately measured by placing a shunt resistance in series with a PZT actuator and measuring the voltage drop across it [15]. The charge is then calculated by integrating the current over time.

$$q(t) = \frac{1}{R}\int_0^t V_s d\tau \tag{25}$$

$q(t)$ is the charge on the PZT actuator at time t, R is the shunt resistance, and v_s is the measured voltage across the resistance. Figure 9 shows the circuit used to measure charge. V is the driving voltage from the amplifier and R is the shunt resistance. An instrumentation amp measures the voltage drop across the shunt resistor. An instrumentation amp measures a differential voltage with a high impedance input on both the positive and negative terminals and low impedance at the output. This ensures minimal interaction between data acquisition hardware and the PZT actuators. It also ensures that the data acquisition hardware measures a low impedance source, which will give the best accuracy [22]. The relay allows the leads of the PZT actuators to be shorted to ground. Hysteresis is dependent on initial conditions [18]. Shorting the leads allows a consistent initial condition to be established so that hysteresis modeling will be more accurate.

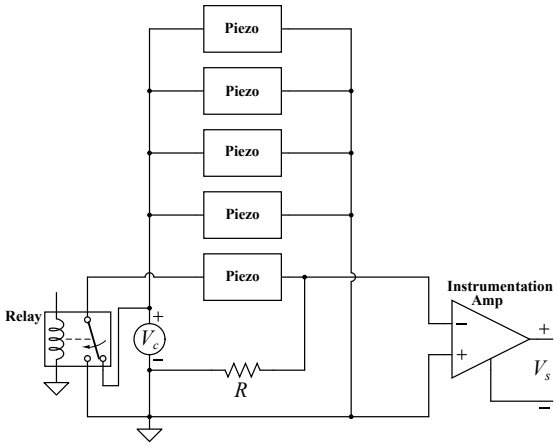

Fig. 9. Charge Measurement Circuit

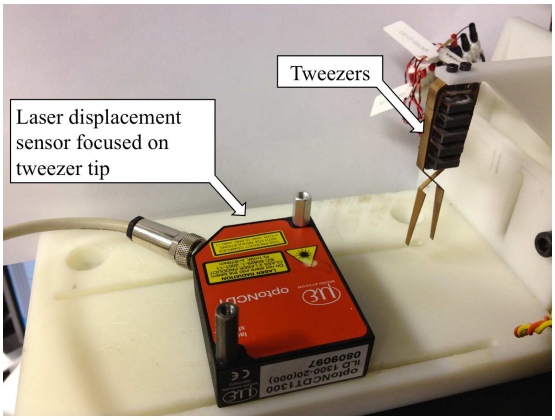

Fig. 10. Experimental setup for displacement sensing

To assess the force and displacement self-sensing two experimental setups are used. Though the self-sensing technique can estimate force and displacement simultaneously, they are evaluated separately here because it simplifies taking the reference measurement. For displacement, a Micro-Epsilon OptoNCDT 1300 Laser Displacement sensor with a range of 20 mm and resolution of 4 µm is used as a reference measurement. The experimental setup is shown in Fig. 10. To measure the force at the tip a Futek LSB200 load cell with a range of 1 N and 0.1% accuracy of is used, with an Omega DRG-SC-BG signal conditioner. The experimental setup is shown in Fig. 11 For both cases a National Instruments USB 6229 was used to measure V_s and to output the control signal to the amplifier. Data was recorded at 1000 Hz, and the resolution was 162 µV for all measurements.

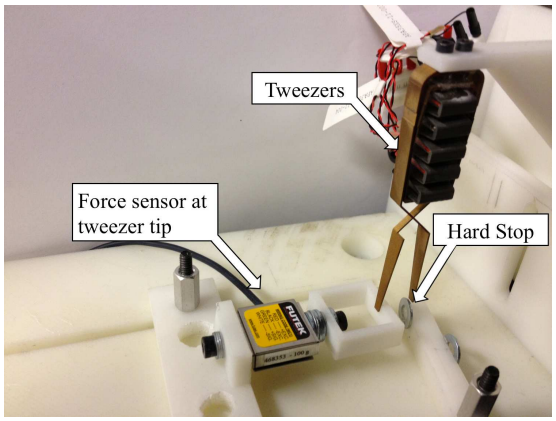

Fig. 11. Experimental setup for force sensing

TABLE II
PERFORMANCE OF SELF-SENSING TECHNIQUE

Performance of Self-Sensing Technique			
Measurement	Mean Error	Mean Error Reported by Kurita et al. [6]	Mean Error Reported by Badel et al. [15]
Displacement	0.4 mm (12%)	0.39 mm (11%)	0.69 µm (2%)
Force	0.012 N (12%)	0.086 N (11%)	20 N (2%)

B. Experiments and Results

Force and displacement self-sensing were tested under a variety of loading conditions from fully blocked tweezer tips to fully free, as well as with various sizes of rigid objects used as a disturbances. First, the hysteresis operator H(q) was calibrated using data from the free case. Figure 12 shows the calibrated operator hysteresis $H(q)$. Fifteen elementary play, superpostion, and creep operators were used. $H(q)$ shows a good match to the experimental data, with a maximum error of 3.34 V and an average error of 0.81 V, or 2.4% and 0.58% respectively of the output range. If the actuator is discharged before reaching it's maximum charge capacity minor loops will form. Also, note that charge is now the independent variable, as dictated by the model in Fig. 7.

Table II summarizes the performance of the self sensing technique. Figures 14 and 15 show the self-sensed displacement and force versus the reference measurement for a variety of loading conditions. Note these figures show the estimation of $\Delta x_{pzt}/2$ since the laser sensor measures only one side of the tweezers. The displacement of the other side is assumed to be identical. Two simple techniques were implemented to slightly increase the accuracy. The force and displacement measurements were limited to their respective maximum and minimum values. Additionally, for the displacement measurement slight drift was removed with a sliding DC offset. The offset reset as the current displacement measurement whenever the input voltage was zero. Figure 13 shows the effect of these techniques. Two input signals were used, one purely sinusoidal and one a mixture of trapezoidal and sinusoidal inputs. The pure sinusoidal input was also used in the calibration of the hysteresis operator. The average accuracy of the self-sensed measurement is 12% of the dynamic range.

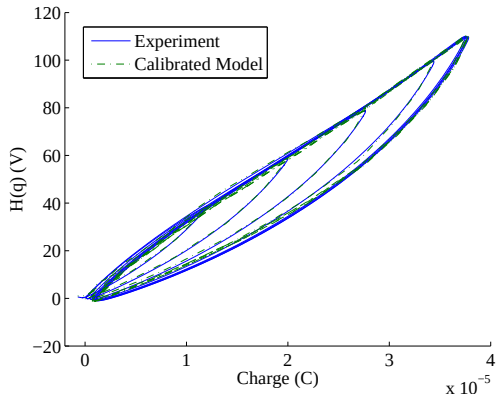

Fig. 12. Hysteresis operator $H(q)$ calibration. The loop is traversed clockwise with increasing charge. Minor loops form if less charge is collected on the actuator when it discharges.

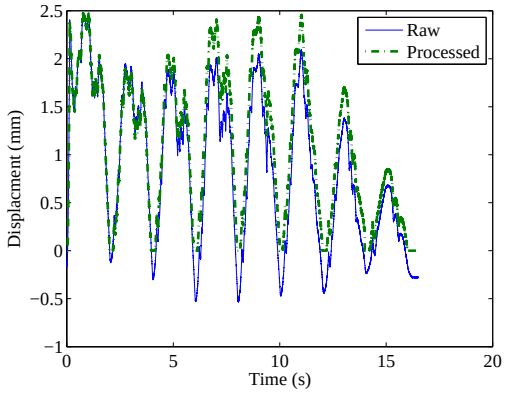

Fig. 13. Effect of Limiting and Sliding DC Offset

VI. DISCUSSION

Though error is present, the accuracy of the self-sensing method is comparable to that reported Kurita, et al. in an earlier study of the same device [6]. However, the sensing method developed in that work relied on prior knowledge of the loading condition as either fixed or free. Due to the constant boundary conditions, i.e. fully blocked tip, the force (or displacement) at the tip depends only on the measured charge. Since hysteresis is generally not observed between charge and force (or displacement), the sensing accuracy is limited only by the charge measurement. The method presented here has lower accuracy but extends the sensing capability to situations with unknown tip conditions. This is beneficial since in many applications the condition at the tip cannot be known a priori. To meaningfully compare the accuracy between different studies, the accuracy as a percent of the full scale output should be compared. Note that the absolute error reported here is lower than that in [6]. This is due to the fact that the version of the tweezers used in this study produced less output force due to manufacturing difficulties. If more output force was produced the measurement would be scaled up, but the signal to noise ratio of the charge and voltage measurements would remain the same. Since the noise would be scaled up as well the error as a percentage of full

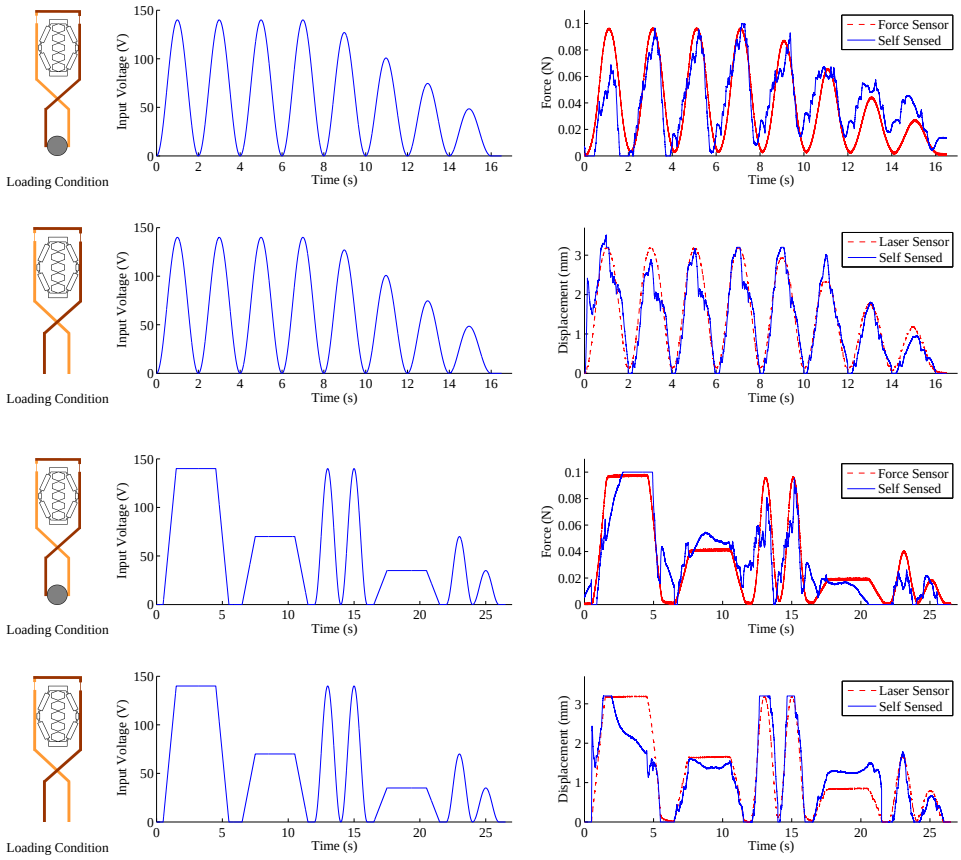

Fig. 14. Blocked Force and Free Displacement

scale output should remain the same.

The accuracy reported here is lower than that reported by Badel et al. in [15], where a similar method was used but for a solitary PZT actuator. There are several possible causes of error. First, the tweezers mechanism is very compliant. This means that a large change in displacement at the tip corresponds to a small change at the PZT actuator. Consider the simple mechanical system in Fig. 16, which represents a PZT actuator in series with a stiffness and serves to illustrate the effect in question. If the endpoint is free, the displacement of the midpoint is

$$\Delta x_{pzt} = \frac{f_{pzt}}{k_{pzt}} \tag{26}$$

If the endpoint is blocked the displacement becomes

$$\Delta x_{pzt} = \frac{f_{pzt}}{k_{pzt} + k_1} \tag{27}$$

If k_1 is small relative to k_{pzt} the displacements in the blocked and free cases will be very close to each other. The tweezer mechanism is more complicated than the system in Fig. 16, but the basic effect is the same, namely the displacement of the displacement of the PZT actuator will not vary much between the blocked and free cases. Charge is directly related to the displacement on the actuator and the applied voltage, based on (4). This means that for the same driving voltage a small change in the displacement, and subsequently charge, will cover the entire range of loading conditions at the tip. In effect, the signal to noise ratio is drastically worsened, meaning that not only the charge and voltage measurements but also the hysteresis model must be extremely accurate.

In fact, despite the less than 1% average error of the hysteresis model, this mismatch is likely the main cause of error. The force predicted by the self-sensing technique in the free case shows the effect of mismatch in the hysteresis model since this is the calibration case for the hysteresis operator. Therefore the effect of the mismatch on force prediction can be shown by subtracting this case from any other, given the same input voltage. Figure 17 shows a self-sensed force measurement, and the same measurement when the error due to model mismatch has been subtracted. This significantly improves the measurement, indicating that despite its relatively low error the hysteresis operator is the main limiting factor of accuracy, rather than charge or voltage measurement. This indicates that for a robot with a set of prepregrommed motions, the model error could be calculated in advance and used to improve the sensing accuracy. For example, if the tweezer end effector was controlled by the push of a button to toggle between open or closed, the self sensing method could be used to obtain useful information such as the size of a grasped object. If the command is not known in advance, increasing the number elementary operators in the hysteresis model could provide a slight increase in accuracy, but this becomes computationally

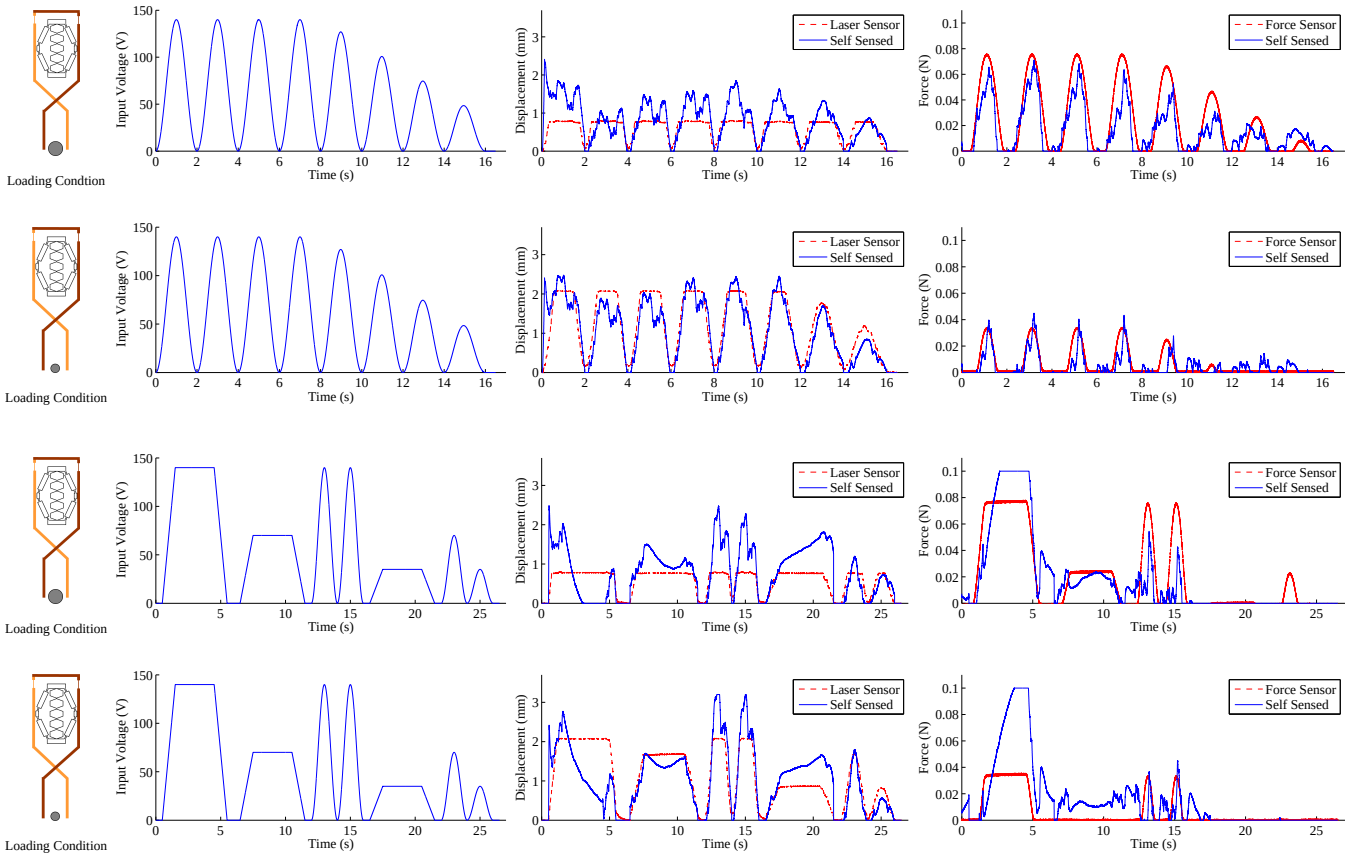

Fig. 15. Intermediate Loading Conditions

intensive and will reach a point of diminishing returns. Additionally, the creep effect is another source of error. Prior work on self sensing, even those assuming quasistatic operation, has been limited to a time scale of milliseconds, over which the effect of creep is negligible. For a robotic end effector the time scale of interest is seconds or minutes, at which point creep can no longer be ignored.

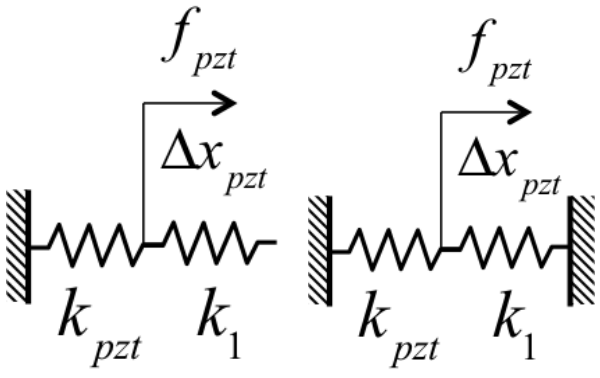

(a) Free (b) Blocked

Fig. 16. A simple model of a PZT actuator and a stiffness in series

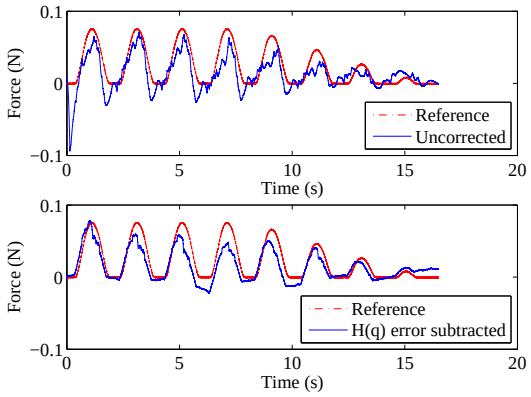

Fig. 17. The effect of hysteresis model mismatch on accuracy

VII. Conclusion

A self-sensing technique has been developed that allows the force and displacement of a tweezer style end effector to be simultaneously estimated if voltage and charge are measured. This technique relies on a hysteretic piezoelectric model and two port network modeling of nested strain amplification mechanisms. Additionally, an on site calibration procedure was developed that does not require specific loading conditions on the piezo actuator. By making a simplifying assumption the hysteresis operator characterizing the system can be calibrated

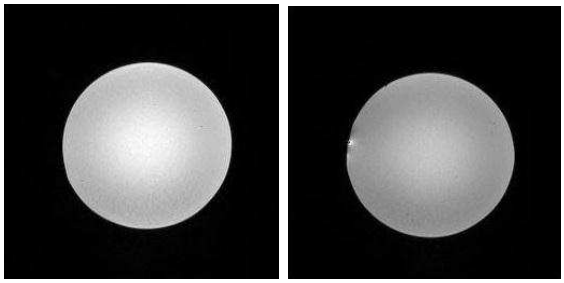

(a) Reference (b) Tweezer Device in Chamber

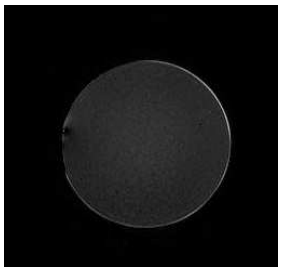

(c) Difference between reference and tweezer test

Fig. 18. Static test of tweezers' effect on MRI image quality

with an experiment requiring an unloaded tweezer tip. Once the hysteresis operator is known other model parameters are easily identified by regression. The modified Prandtl-Ishlinksii approach was used to model hysteresis. Despite the method's accuracy, it was seen that hysteresis model mismatch was a major cause of error, due to the highly compliant tweezer structure. The force and displacement measurements were seen to have an average error of 12%, comparable to the much more limited method in [6]. Potential future work in this area could involve development of more advanced signal processing techniques to improve the accuracy of the estimation, as well extending the applicability of the sensing method to the dynamic case.

APPENDIX A
MATERIAL SELECTION

To ensure MRI compatibility the device must be constructed with materials of sufficiently low magnetic susceptibility. As a ceramic, PZT is relatively unaffected by magnetic fields. The metal amplification structure of the Cedrat APA35XS actuators are titanium. This is a non-standard option, but is readily available from the manufacturer. The tweezer structure itself is machined from phosphor bronze. Both titanium and phosphor bronze have relatively low magnetic susceptibility and are considered safe to use in MRI environments [23].

MRI compatibility encompasses two main ideas. First, the device should experience forces and torques within the MRI chamber that are low enough to be negligible. Second, the imaging should be degraded as little as possible [23]. A static test was performed to asses the MRI compatibility of the device. As expected, the device was not significantly affected by the magnetic fields. The effect on the image quality is shown in Fig. 18. The images show a round ball in the MRI chamber. The tweezers create slight distortion of the image. Additionally the signal to noise ratio of the image is lowered slightly from 22.84 to 21.08. In general the image distortion is not severe. Though only a static test was performed, piezoelectrically driven devices constructed of titanium have been tested by Cedrat and were shown to produce acceptable levels of image distortion [24]. Other studies have also shown piezoelectrically driven actuators will produce low levels of noise and distortion with appropriate shielding of the driving electronics [25] [26]. This indicates that the device could be likely be used in the MRI environment, though a dynamic test is needed to fully assess the device's impact on the MRI image quality.

ACKNOWLEDGMENT

The authors wish to thank the Korea Institute for Advancement of Technology (KIAT) for their sponsorship of this research.

REFERENCES

[1] D. Gerhardus, "Robot-assisted surgery: The future is here," *Journal of Healthcare Management*, vol. 4, pp. 242–251, 2003.

[2] V. Seifert, M. Zimmerman, C. Trantakis, H.-E. Vitzhum, K. Kuhnel, A. Raabe, F. Bootz, J.-P. Schnieder, F. Schmidt, and J. Dietrich, "Open MRI-guided neurosurgery," *Acta Neurochirurgica*, vol. 141, pp. 455–464, 1999.

[3] K. Hynynen, A. Darkazanli, E. Unger, and J. Schenck, "MRI-guided noninvasive ultrasound surgery," *Medical Physics*, vol. 20, pp. 107–115, 1992.

[4] F. Jolesz, A. Nabavi, and R. Kikinis, "Integration of interventional MRI with computer-assisted surgery," *Journal of Magnetic Resonance Imaging*, vol. 13, pp. 69–77, 2001.

[5] E. McVeigh, M. Guttman, R. Lederman, M. Li, O. Kocaturk, T. Hunk, S. Kozlov, and K. Horvath, "Real-time interactive MRI-guided cardiac surgery," *Magnetic Resonance in Medicine*, vol. 56, pp. 958–964, 2006.

[6] Y. Kurita, F. Sugihara, J. Ueda, and T. Ogasawara, "Piezoelectric tweezer-type end-effector with force and displacement sensing capability," *IEEE/ASME Transactions on Mechatronics*, vol. 17, no. 6, pp. 1039–1048, December 2012.

[7] J. J. Dosch, D. J. Inman, and E. Garcia, "A self-sensing piezoelectric actuator for collocated control," *Journal of Intelligent Material Systems and Structures*, vol. 3, pp. 166–185, 1992.

[8] J. Garnett E. Simmers, J. R. Hodgkins, D. D. Mascarenas, G. Park, and H. Sohn, "Improved piezoelectric self-sensing actuation," *Journal of Intelligent Material Systems and Structures*, vol. 15, pp. 941–953, 2004.

[9] S. Kuiper and G. Schitter, "Active damping of a piezoelectric tube scanner using self-sensing piezo actuation," *Mechatronics*, vol. 20, pp. 656–665, 2010.

[10] I. A. Ivan, M. Rakotondrabe, P. Lutz, and N. Challiet, "Current integration force and displacement self-sensing method for catilevered piezoelectric actuators," *Review of Scientific Instruments*, vol. 80, pp. 126 103–1–126 103–3, 2009.

[11] ——, "Quasistatic displacement self-sensing method for cantilevered actuators," *Review of Scientific Instruments*, vol. 80, 2009.

[12] N. Ohta, K. Furutani, and Y. Mieda, "Displacement monitoring of stacked piezoelectric actuator by observing induced charge," in *Proceedings of the 1st International Conference on Positioning Technology*, 2004.

[13] M. Goldfarb and N. Celanovic, "A lumped parameter electromechanical model for describing the nonlinear behavior of piezoelectric actuators," *ASME Jornal of Dynamic Systems, Measurement, and Control*, vol. 119, pp. 478–485, 1997.

[14] H. M. Georgiou and R. B. Mrad, "Electromechanical modeling of piezoceramic actuators for dynamic loading applications," *ASME Jornal of Dynamic Systems, Measurement, and Control*, vol. 128, pp. 558–567, 2006.

[15] A. Badel, J. Qiu, and T. Nakano, "Self-sensing force control of a piezoelectric actuator," *IEEE Transactions on Ultrasonics, Ferroelectrics and Frequency Control*, vol. 55, pp. 2571–2581, 2008.

[16] J. Ueda, T. W. Secord, and H. H. Asada, "Large effective-strain piezoelectric actuators using nested cellular architechture with exponential strain amplification mechanisms," *IEEE/ASME Transactions on Mechatronics*, vol. 15, pp. 770–782, 2010.
[17] K. Kuhnen, "Modeling, identification,and compensation of complex hysteretic nonlinearities a modified Prandtl-Ishlinskii approach," *European Journal of Control*, vol. 9, pp. 407–418, 2003.
[18] M. Brokate and J. Sprekels, *Hysteresis and Phase Transistions*, J. Marsden, L.Sirovich, and F. John, Eds. Springer, 1996.
[19] R. Banning, W. L. de Koning, H. J. Adriaens, and R. K. Koops, "State-space analysis and identification for a class of hysteretic systems," *Automatica*, vol. 37, pp. 1883–1892, 2001.
[20] K. Kuhnen, "Modeling, identification, and compensation of complex hysteretic and log(t)-type creep nonlinearities," *Control and Intelligent Systems*, vol. 33, pp. 134–147, 2005.
[21] "Cedrat technologies piezo products catalouge," 2011.
[22] *DAQ M Series Manual*, National Instruments Corporation, 11500 North Mopac Expressway, Austin, TX 78759, USA, July 2008.
[23] J. Schenck, "The role of magnetic susceptibility in magnetic resonance imaging: MRI magnetic compatibility of the first and second kinds," *The International Journal of Medical Physics*, vol. 23, pp. 815–850, 1995.
[24] C. Belly, H. Mathieu, F. Claeyssen, and R. L. Letty, "MRI-compliant micro-motors for medical and biomedical applications," Cedrat Technologies, Tech. Rep., 2010.
[25] K. Chinzei, R. Kikinis, and F. Jolesz, "MR compatibility of mechatronic devices: Design criteria," in *Proceedings of Medical Image Computing and Computer-assisted Intervention*, 1999.
[26] Y. Wang, G. Cole, H. Su, J. Pilitsis, and G. Fischer, "MRI compatbility evaluation of a piezoelectric acutator system for a neural interventional robot," in *Proceedings of the 31st Annual International Conference of the IEEE EMBS*, 2009.

Timothy McPherson Timothy McPherson received the B.S. and M.S. degrees in Mechanical Engineering from the Georgia Institute of Technology in 2010 and 2012. He is currently with the Control Algorithms Group, Extreme Ultraviolet Lithography Light Source Division, Cymer, San Diego, CA.

Jun Ueda Jun Ueda (M01) received the B.S., M.S., and Ph.D. degrees from Kyoto University, Kyoto, Japan, in 1994, 1996, and 2002, respectively, all in mechanical engineering. From 1996 to 2000, he was a Research Engineer with the Advanced Technology Research and Development Center, Mitsubishi Electric Corporation, Hyogo, Japan. From 2002 to 2008, he was an Assistant Professor with the Graduate School of Information Science, Nara Institute of Science and Technology, Nara, Japan. From 2005 to 2008, he was a Visiting Scholar and Lecturer with the Department of Mechanical Engineering, Massachusetts Institute of Technology, Cambridge. Since 2008, he has been with the George W. Woodruff School of Mechanical Engineering, Georgia Institute of Technology, Atlanta, as an Assistant Professor. His current research interests include vibration control, robust control, mechanical design, and biologically inspired robotics. Dr. Ueda is a co-recipient of the 2009 IEEE Robotics and Automation Society Early Academic Career Award.